Chapter 1

Physical Models for Resistive Switching Devices

Luis-Miguel Procel-Moya

Additional information is available at the end of the chapter

http://dx.doi.org/10.5772/intechopen.69025

Abstract

We present a classification and description of the principal resistive switching and transport mechanisms in chalcogonides materials. We classify the model according to how many material dimensions are involved in the resistive switching mechanism. In this way, we describe the phase change model (3D), the interface modulation model (2D) and models where the switching mechanism depends on the formation of a conduction filament (1D). Among the conduction filament models, we include the thermochemical oxygen diffusion mechanism, the oxidation/reduction mechanism and the quantum point effect.

Keywords: chalcogonides, resistive switching, physical models

1. Introduction

Typically, a resistive switching material changes its resistance between two states: High Resistive State (HRS or OFF-state) and Low Resistive State (LRS or ON-state). The most common structure for a resistive switching devices is an insulator between two metals or metal/insulator/metal (MIM) structure. One of the most important applications of these kind of devices is for non-volatile memories or Resistive RAMs (ReRAMs).

The metal elements of the MIM structure are called top and bottom electrodes. An electrical stimulus is necessary to apply between these electrodes to change the resistive state of the insulator material. In order to determine the resistive state (HRS or LRS), a low voltage is applied on the electrodes, and the current, which flows through the insulator, is measured (I_{HRS} or I_{LRS}). There are several orders of magnitudes of difference between I_{HRS} and I_{LRS} currents. The change from the HRS to the LRS is called SET process and the change from the LRS to the HRS is called RESET process.

Depending on the voltage polarity applied on the electrodes, there are two schemes to change the resistive state: unipolar and bipolar. On the one hand, in the unipolar scheme, the resistive state change does not depend on the voltage polarity and there are two threshold voltages: one

for the RESET process (V_{RESET}) and one for the SET process (V_{SET}) with the same polarity as we can see in **Figure 1**. On the other hand, in the bipolar scheme, V_{RESET} and V_{SET} have different polarities (**Figure 2**).

There is no universal theory or model which explains the electron conduction in the two resistive states and the SET and RESET processes because there are many factors that affect the switching behaviour, such as the type of the insulator material, fabrication process, nature of the dielectric breakdown, among others. However, Waser and Wutting proposed a classification based on the type of the resistive switching mechanisms, such as nanochemical materials, ferroelectric tunnelling, electrostatics effects, phase change mechanism, thermochemical mechanism, redox-based effect, electrochemical effect, molecular switching effect and magnetoresistive effect [1].

Chalcogonides are one of the most used materials in the fabrication of resistive memory devices. The switching mechanisms related to these materials are: phase change memory effect, thermochemical memory effect, redox-based memory effect and interface defect modulation. The phase change mechanism affects the complete volume of the insulator material and it is considered as a 3D mechanism. A 2D resistive switching mechanism is the modulation of the defect density at the metal/insulator interface. Finally, when the resistivity material depends on the formation of a conduction filament (CF), 1D mechanisms are involved in the resistive switching process. Thermochemical diffusion of oxygen, reduction/oxidation of the CF and quantum point contact effects are typical 1D mechanisms.

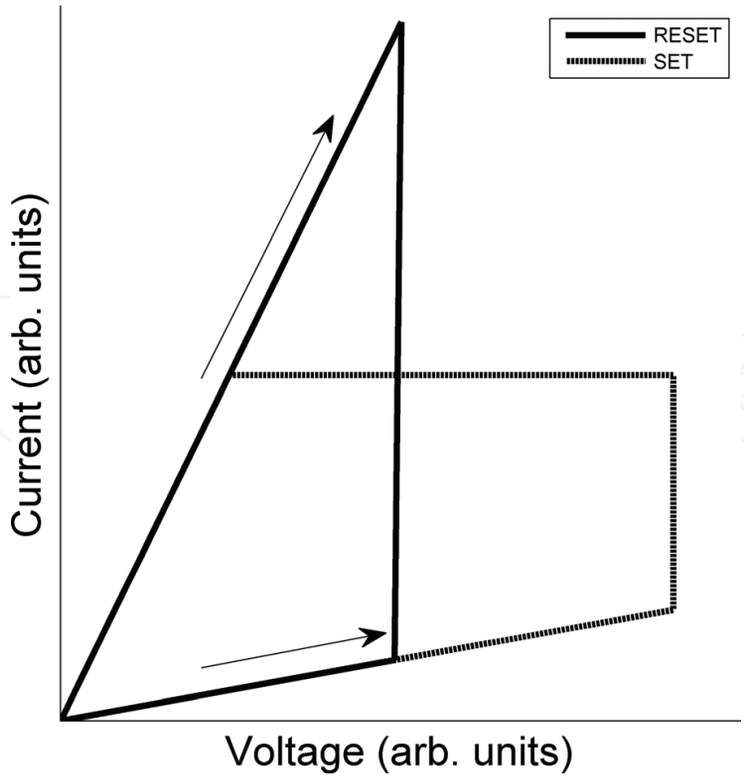

Figure 1. SET and RESET process for unipolar behaviour.

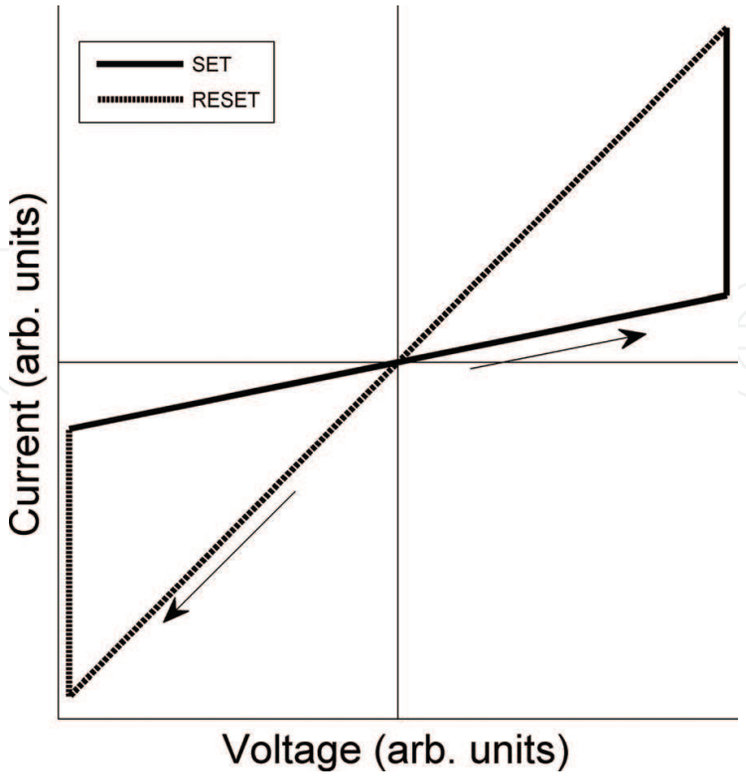

Figure 2. SET and RESET process for bipolar behaviour.

2. Phase change model

Heavier chalcogonides, such as tellurides and selenides, show different electrical and optical properties in their amorphous and crystalline phases (**Figure 3**). The resistive switching of these materials is unipolar. On the one hand, the amorphous phase of these materials has high resistivity and low reflectivity and, on the other hand, crystalline phase has low resistivity and high reflectivity [2]. These properties are being exploited in the development of optical storage

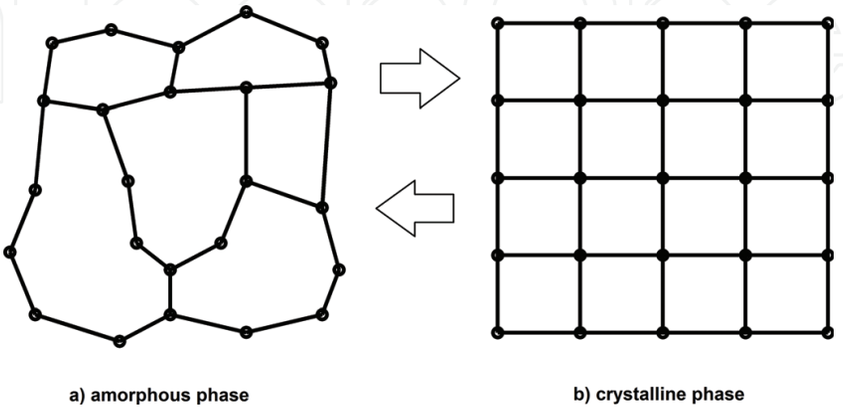

Figure 3. Phase change mechanism: the phase material changes from (a) amorphous phase to (b) crystalline phase (and vice versa) to have different resistivity and reflectivity.

products, such as compact disks (CD), digital versatile disks (DVD), high-definition digital versatile disks (HD-DVD) and Blu-ray disks (BR). The first kind of materials used for optical storage were good glasses, such as Te-based alloys like $Te_{85}Ge_{13}$ doped with Sb, S and P. These materials show good electrical switching properties in the amorphous and crystalline phases but the crystallization time was in the order of microseconds, too high to be considered for optical storage. The second generation of these materials shows shorter crystallization time and good optical properties. Among these materials, we have GeTe, $Ge_{11}Te_{80}Sn_4Au_{23}$, GeTe-$Sb_2Te_3$, GeBiTe and GeInSbTe. After, a third family of materials was later discovered which includes alloys of Sb_2Te doped with Ag, In and Ge [2].

There are two important temperature thresholds in these materials: the melting temperature (T_m) and the glass-transition temperature (T_g) with $T_m > T_g$. The process to change the material phase from crystalline to amorphous and vice versa is as follows [2]:

- To write a bit, a short high-pulse laser or current is applied on the crystalline material to reach T_m temperature.
- The material is cooling down rapidly with a rate higher than 10^9 K/s. In a very short time, the material reaches the amorphous phase without passing through the crystalline one.
- To erase the bit, a long short-pulse laser or current is applied on the amorphous material. The material temperature increases over T_g. There is an increment of the electron mobility and the material changes to the crystalline phase.

For electrical storage devices, the resistive switching property is fundamental and all these materials have it. However, not all these materials have the reflectivity switching property. To have this property, a very short time (few tens of nanoseconds) is needed for cooling down the material from the liquid phase to amorphous phase (step 2) [2].

When a low voltage is applied to the material in the amorphous phase, a very low current is measured due to the high resistance. When the voltage reaches a value around 0.7 V, the resistivity decreases and the material reach the so-called ON-amorphous phase [1, 2]. In these phases, the current increases significantly and enables enough heat to recrystallize the material. During the phase change, material defects play an important role. In the amorphous phase, the current is controlled by the Pool-Frenkel conduction, where carriers are trapped in defect sites according to the following equation (electron hopping mechanism) [1]:

$$I = 2qAN_T \frac{\Delta z}{\tau_0} e^{-(E_C - E_F)/kT} \sinh\left(\frac{qV\Delta z}{2kTt_h}\right) \tag{1}$$

where A is the contact area, V the applied voltage, N_T the integral of the trap distribution, Δz the intertrap distance, τ_0 the scape time for a trapping electron, E_F the Fermi energy, E_C the conduction band energy, q the elementary electron charge and t_h the thickness of the material. Because of the total conduction is presented in the complete material volume, this mechanism is called 3D. Experimental results show that the defect density in the material is very high and most of the defects are negative U-centres [1]. On the other hand, computational simulations show that in the crystalline phase, vacancy defects predominate with a concentration of 25% [1].

3. Metal/insulator interface modulation model

In this model, the resistive switching is presented at the metal/insulator interface. In other words, there is a contact resistance switching behaviour. This interface depending mechanism is presented in Peroskite oxides in which the material resistivity strongly depends on the interface area and the switching mechanism is always bipolar. A typical material that shows this behaviour is the Nb-doped $SrTiO_3$ [3].

The origin of this resistivity change can be understood by examining the metal/insulator interface band diagram as shown in **Figure 4**. The insulator oxide is usually doped with different metals. Depending of doped metal and its density, the insulator behaves as semiconductor at the interface. This provokes a Schottky barrier contact instead of a pure ohmic contact [3].

An electric field applied on the metal electrodes can electrochemically modify the oxygen vacancy density at the interface. For an n-type semiconductor, an increment of the oxygen vacancies density reduces the depletion layer, W_d, in the energy band diagram provoking an increment of the tunnel electron conduction and, therefore, a decrement of the contact

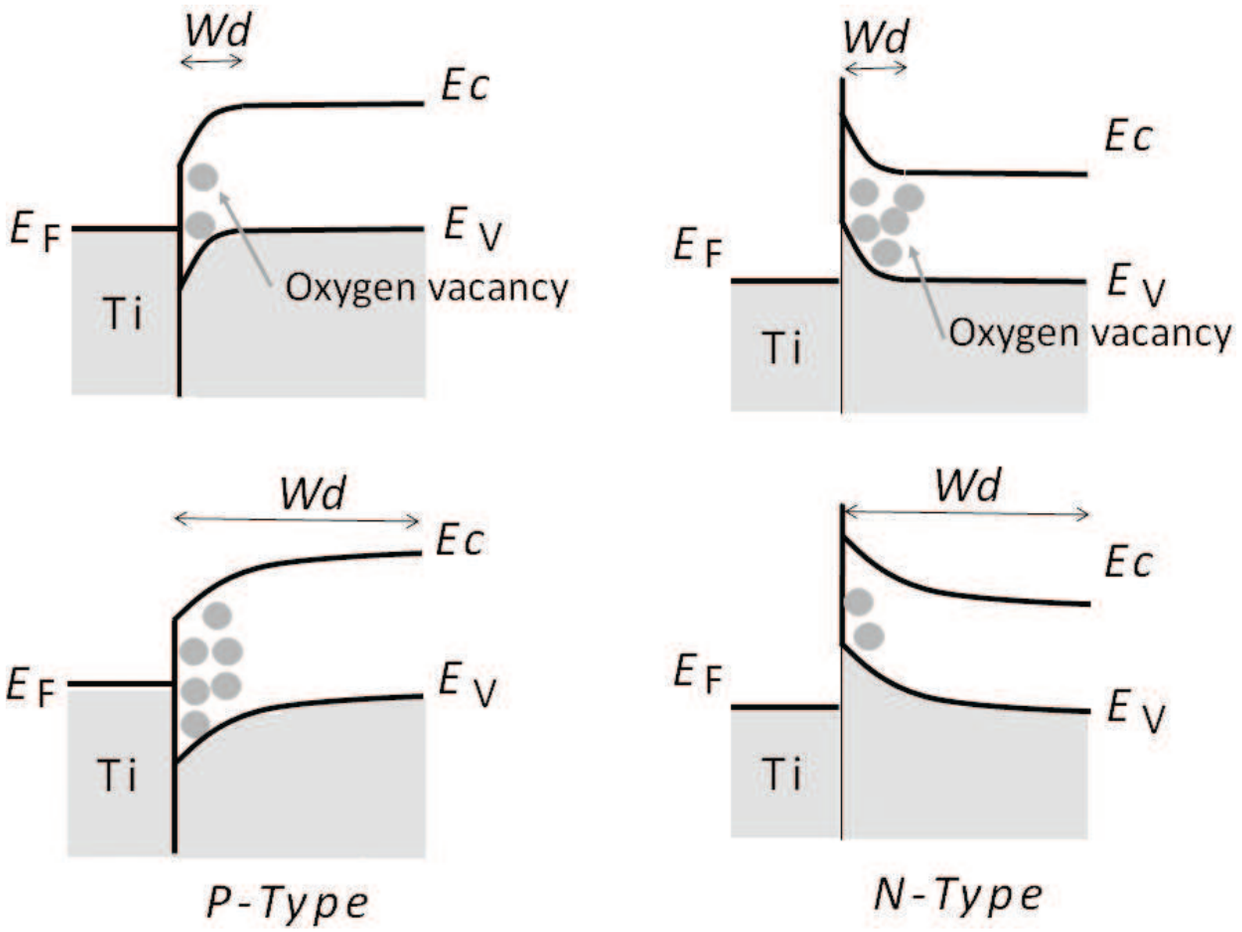

Figure 4. Band diagrams at the Metal/Insulator interfaces. For a p-type semiconductor, the presence of oxygen vacancies increases W_d. For an n-type semiconductor, the presence of oxygen vacancies decreases W_d.

resistance (LRS). If an electric field is applied on the opposite direction, the number of oxygen vacancies in the n-type semiconductor decreases and provokes an increment of W_d and, therefore, the contact resistance increases (HRS). On the other hand, for a p-type semiconductor, the increment of oxygen vacancies increases W_d and the contact resistance (HRS), and a diminution of the oxygen vacancies decreases W_d and the contact resistance (LRS). In this model, the metal work function plays a very important role because the band bending strongly depends on this parameter.

Sawa showed very good resistive switching results for Ti/$Pr_{07}Ca_{0.3}MnO_3$/$SrRuO_3$ (Ti/PCMO/SRO) cells, where SRO has metal properties and PCMO acts as p-type semiconductor. As well, the SRO/$SrTi_{0.99}Nb_{0.01}O_3$/Ag (SRO/Nb:STO/Ag) cell showed a good resistive switching behaviour where Nb:STO acts as an n-type semiconductor [3].

Another way to change the contact resistance is by adding a thin semiconductor layer of an oxide material between the metal and the insulator materials [3]. The semiconductor layer transforms the contact resistance from ohmic to a Schottky barrier. Without this layer, there is no switching resistance for some insulators. Sawa shows experimental results for Ti/$Sm_{0.7}Ca_{0.3}MnO_3$(n unit cells)/$La_{0.7}Sr_{0.3}MnO_3$/SRO (Ti/SCMO(n)/LSMO/SRO) where SCMO is a p-type semiconductor [3]. It was demonstrated that for n = 5 unit cells, there was a very good hysteresis in the I-V curve. As well, the SRO/$SrTiO_3$/$SrTi_{0.99}Nb_{0.01}O_3$/Ag (SRO/STO/Nb:STO) cell showed a resistivity changes but not a good hysteresis in the I-V curve [3].

4. One dimensional models for resistive switching materials

In several transition metal oxides, when a voltage is applied on the electrodes of a pristine MIM cell, the current measured is very low. When the voltage increases up to a threshold value, the electric field applied provokes a dielectric breakdown. When this occurs, a conduction filament (CF) is formed in the insulator as shown in **Figure 5**. The necessary potential to form this filament is called forming voltage (V_F). The CF is formed due to the Joule-heating effect, which leads a temperature increment in the insulator. The dielectric breakdown is driven by a thermal runway. When a voltage is applied on a transition metal oxide, the resistance

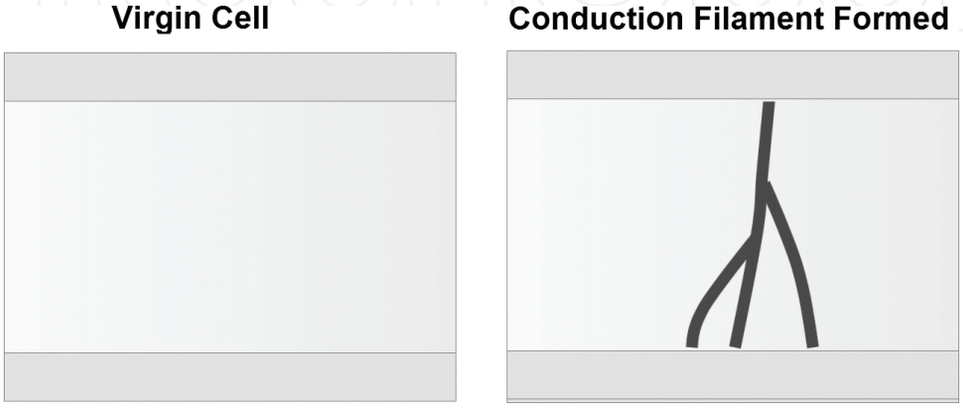

Figure 5. Left: virgin cell. Right: Cell with conduction filament formed.

starts to decrease but not in a permanent way. In this process, the material temperature increases up to certain value (related to a threshold voltage) when a local redox reaction begins and causes structural defects (grain boundaries or dislocations) [4].

The voltage polarity to change states in cells with CF can be unipolar or bipolar. For unipolar behaviour, the electron conduction mechanism is related to thermochemical changes in the filament due to the Joule-heating effect. On the other hand, for bipolar behaviour, the electron conduction through the CF depends on redox effects or quantum point contact effects. In both cases, the switching mechanisms (SET and RESET processes) are related to the thermochemical oxygen diffusion in the CF. We can consider the CF as a 1D parameter because the material resistivity is area independent. It is very important to note that in CF programmable devices, there exist a variability problem because not all filaments are equal or similar [5].

4.1. Thermochemical oxygen diffusion model

Ielmeni, Nardi and Cagli have been developed a physical model for NiO cells with very good concordance with experimental results [4]. In this material, the RESET process happens in small steps, whereas the change of states occurs suddenly during the SET process. The $V_{\mathrm{RESET}}$and I_{RESET} parameters depend on the resistance material in the HRS. I_{RESET} always decreases when the resistance increases. On the other hand, the V_{RESET} in function of R curve has an U behaviour. That is, for low values of R, V_{RESET} decreases when R increases, and for high values of R, V_{RESET} increases when R increases. For the RESET process, the CF temperature depends on the square of the applied voltage as follows [4]:

$$T = T_0 + \frac{R_{\mathrm{th}}}{R} V^2 \tag{2}$$

where T_0 is the room temperature and R_{th} is the effective thermal resistance. By using Eq. (2), we can obtain the V_{RESET} voltage:

$$V_{RESET} = \sqrt{\frac{R\Delta T_{RESET}}{R_{th}}} \tag{3}$$

where $\Delta T_{\mathrm{RESET}}$ is the critical temperature increment for the onset oxidation. The ratio R/R_{th} is almost constant according to the Wiedemann-Franz law for metals [4]. This means that V_{RESET} is almost constant and I_{RESET} decreases with respect to R. This is not true in experimental results. For explaining the increment of V_{RESET} with respect to high values of R, we have to study the size-dependent Joule-heating effect. The parameter R_{th} is the parallel of two resistances: $R_{\mathrm{th}}{}'$ and $R_{\mathrm{th}}{}''$, where $R_{\mathrm{th}}{}'$ only depends on the CF and $R_{\mathrm{th}}{}''$ depends on the rest of the material (bulk oxide). $R_{\mathrm{th}}{}'$ can be computed by considering the thermal nanofilament conductivity, k_{th}, as follows [4]:

$$R_{\mathrm{th}}{}' = \frac{t_h}{8k_{\mathrm{th}}A_{\mathrm{CF}}} \tag{4}$$

where t_{h} is the oxide thickness and A_{CF} is CF area. As R_{th} is inverse proportional to A_{CF}, for high values of A_{CF} (low resistance) R_{th} is approximately $R_{\mathrm{th}}{}'$. On the other hand, for low values of ACF, we have that $R_{\mathrm{th}} \approx R_{\mathrm{th}}{}''$. As well, when k_{th} increases, $R_{\mathrm{th}}{}'$ predominates over $R_{\mathrm{th}}{}''$.

For explaining the behaviour of the V_{RESET}-R curve for low values of R, we have to consider that the ratio R/R_{th} is almost constant in Eq. (3) and $\Delta T_{\mathrm{RESET}}$ must increase in order to obtain a metal diffusion in the filament, which is a filament area dependent process. Hence, V_{RESET} increases for low values of R. This size-dependent diffusion is considering in following Arrhenius expression developed in Ref. [4]:

$$T_{RESET} = \frac{E_A}{k\log\left(\frac{t_{RESET}}{t_0}\left(\frac{\varphi_0}{\varphi}\right)^2\right)} \tag{5}$$

where E_{A} is the activation energy, k the Boltzmann constant, t_0 and ϕ_0 are constants, ϕ is the CF diameter and t_{RESET}= 1s is the reset time. Ielmini et al. showed very good results between their model and experimental data of NiO devices [4].

The electron conduction mechanism in the LRS strongly depends on the activation energy. For low values of E_{A}, the filament has a metallic behaviour and the resistance is given by:

$$R = R_{0m}(1 + \alpha(T - T_0)) \tag{6}$$

where T_0 is the room temperature, $R_{0\mathrm{m}}$ is the metallic resistant at T_0 and α is the temperature coefficient. On the other hand, for high values of E_{A}, electron conduction is driven by the Pool-Frenkel model in semiconductors and the resistance follows the following equation:

$$R = R_{0s}\exp\left(\frac{E_{AC}}{kT}\right) \tag{7}$$

where $R_{0\mathrm{s}}$ is the extrapolated resistance at infinite T, k is the Boltzmann constant and E_{AC} is the activation energy for conduction. Both conduction behaviours are related to position of Fermi level (E_{F}). Inside the CF filament, there are oxygen vacancies, whereas the bulk oxide is doped by oxygen. An insulator doped by oxygen behaves as a p-type semiconductor and, on the other hand, oxygen vacancies provoke an n-type behaviour. Therefore, the conduction filament in LRS behaves as an n-type semiconductor and the electron conduction is modulated by the concentration of oxygen vacancies, which is directly related to the E_{F} position. When the oxygen vacancies concentration is too high, the CF behaves as a degenerately doped semiconductor and E_{F} is very close or above the conduction band [4].

As was mentioned before, the SET process happens suddenly and it strongly depends on the resistance of the HRS (before the SET process). The HRS resistance can be described by the Pool-Frenkel model and is given by Ielmini et al. [4]:

$$R = \frac{kT\tau_0 t_h}{q^2 A_{\mathrm{CF}} N_T \Delta z^2}\exp\left(\frac{E_{AC}}{kT}\right) \tag{8}$$

where τ_0 is the attempt-to-escape characteristic time for a carrier from a specific state, t_{h} is the material thickness (or filament length), N_T is the dopant density, A_{CF} is the filament area and Δz is the distance between positive charged defects. Ielmini et al. showed, from experimental

data, that necessary power for the setting process (P_{SET}) is directly proportional to $R^{-0.5}$, which means that [4]:

$$V_{SET} = \frac{P_{SET}}{I_{SET}} = \sqrt{P_{SET}R} \propto R^{0.25} \tag{9}$$

$$I_{SET} = \frac{P_{SET}}{V_{SET}} = \sqrt{\frac{P_{SET}}{R}} \propto R^{-0.75} \tag{10}$$

The tendencies for V_{SET} and I_{SET} parameters in function of R were experimentally confirmed the Ielmini group in Ref. [4].

4.2. Trap-assisted-tunnelling model

In bipolar cells, the transition between the LRS and the HRS is commonly related to the formation and rupture of the CF. A typical material which presents a CF with bipolar behaviour is the HfO_2. As well as in unipolar cells, oxygen vacancies play an important role. The most accepted theory for forming the CF in a virgin cell is that the oxygen atoms migrate from the CF to the insulator/metal interface due to the Joule-heating effect. When the CF is already formed, to change from the LRS to the HRS, the CF is oxidized (oxygen atoms migrate from the electrode to the CF), whereas to change from the HRS to the LRS, the CF is reduced leaving oxygen vacancies and forming percolation paths (oxygen atoms migrate from the CF to the electrode).

Guan, Yu and Wong have developed a model for explaining the carrier conduction through the CF in bipolar cells where the principal transport mechanism is the trap-assisted-tunnelling (TAT). The continuity transport equation in the oxide region is given by Guan et al. [6]:

$$\frac{df_n}{dt} = (1-f_n)\sum_{m=1,\, m\neq n}^{N} R_{mn}f_m - f_n\sum_{m=1,\, m\neq n}^{N} R_{mn}(1-f_n) + (R_n^{iL}+R_n^{iR})(1-f_n) - (R_n^{oL}+R_n^{oR})f_n \tag{11}$$

where f_n is the electron occupation probability of the nth trap, R_{mn} is the electron hopping rate from trap m to trap n, R_n^{oL}/R_n^{oR} are the electron hopping rate from trap n to the right/left electrode and R_n^{iL}/R_n^{iR} the electron hopping rate from the right/left electrode to trap n. It is well known that oxygen vacancies contribute to the TAT. In quasi-steady state, Eq. (11) transform to [6]:

$$(1-f_n)\sum_{m=1,\, m\neq n}^{N} R_{mn}f_m - f_n\sum_{m=1,\, m\neq n}^{N} R_{mn}(1-f_n) + (R_n^{iL}+R_n^{iR})(1-f_n) - (R_n^{oL}+R_n^{oR})f_n = 0 \tag{12}$$

The current can be computed by evaluating the electron flow near the electrode:

$$I = I^L = I^R = -q\sum_{n=1}^{N}\left((1-f_n)R_n^{iL} - f_nR_n^{oL}\right) = -q\sum_{n=1}^{N}\left((1-f_n)R_n^{iR} - f_nR_n^{oR}\right) \tag{13}$$

The hopping rate can be computed by the Mott hopping model as [7]:

$$R_{mn} = R_0 \exp\left(-\frac{r_{mn}}{a_0} + \frac{qV_{mn}^H}{kT}\right) \tag{14}$$

where $R_0 \approx 10^{12}$Hz is the vibration electron frequency, $r_{\mathrm{mn}} = |r_{\mathrm{m}} - r_{\mathrm{n}}|$ is the distance between vacancies n and m, a_0 is the attenuation length wave function, $V_{\mathrm{mn}}{}^{\mathrm{H}} \approx -F^H(r_{\mathrm{m}} - r_{\mathrm{n}}) \approx V^H(r_{\mathrm{m}}) - V^H(r_{\mathrm{n}})$ is the barrier change due to an external electric field and $V^H(r_{\mathrm{n}})$ is the homogeneous component of the potential solution of the Poisson equation. The hopping rates from a trap to an electrode are [6]:

$$\begin{aligned} R_n^{iL,R} &= R^0_{\mathrm{tunnel}} N^{L,R}(E_v^+) F_{\mathrm{in}}^{L,R}(E_v^+) T_n^{L,R,+} \\ R_n^{oL,R} &= R^0_{\mathrm{tunnel}} N^{L,R}(E_v^\bullet) F_{\mathrm{out}}^{L,R}(E_v^\bullet) T_n^{L,R,\bullet} \end{aligned} \tag{15}$$

where e $R^0{}_{\mathrm{tunnel}}$ is the tunnel coupling strength between a trap and an electrode, $N^{L,R}$ is the number of states at a given energy in an electrode and $E_{\mathrm{v}}{}^+/E_{\mathrm{v}}{}^\bullet$ are the energy of an empty/filled trap given by Guan et al. [6]:

$$E_v^{+,\bullet}(r_n) = E_v^{+,\bullet} - qV^H(r_n) \tag{16}$$

$T_n{}^{L,R,+\bullet}$ is the tunnel probability from the left/right electrode into a trap given by the Wentzel-Kramers-Brillouin approximation [6]:

$$\begin{aligned} T_n^{L+,\bullet} &= \exp\left[\int_0^{x_n} \frac{1}{h}\sqrt{2m^*\left[E_C - E_{v0}^{+,\bullet} - qV^H(x_n)\right]}dx\right], \quad E_v^{\pm} < E_C - qV^H(x) \\ T_n^{R+,\bullet} &= \exp\left[\int_{x_n}^{L} \frac{1}{h}\sqrt{2m^*\left[E_C - E_{v0}^{+,\bullet} - qV^H(x_n)\right]}dx\right], \quad E_v^{\pm} < E_C - qV^H(x) \end{aligned} \tag{17}$$

where x_n is the xth component of r_n, L is the oxide thickness and m^* is the tunnelling effective mass in the oxide. $F_{\mathrm{in}}{}^{\mathrm{L,R}}$ is the Fermi integral which represents the filled states in an electrode above $E_{\mathrm{v}}{}^+$ and takes into account the inject electrons from the electrode into the trap n:

$$F_{in}^{L,R}(E_v^+) = \int_{E_{v0}^+ - qV(x_n)}^{+\infty} f\left(E - (E_F^{L,R} - qV^{L,R})\right)dE = \int_{E_{v0}^+ - qV(x_n)}^{+\infty} \frac{1}{1 + \exp\left((E - (E_F^{L,R} - qV^{L,R})/kT\right)}dE \tag{18}$$

where $E_{\mathrm{F}}{}^{\mathrm{L,R}}$ is the Fermi level of the right/left electrode and $V^{L,R}$ is the applied voltage on the left/right electrode. On the other hand, $F_{\mathrm{out}}{}^{\mathrm{L,R}}$ is the Fermi integral which takes into account the number of empty states in an electrode bellow $E_{\mathrm{v}}{}^-$ which can accept electrons from the trap n:

$$F_{out}^{L,R}(E_v^-) = \int_{-\infty}^{E_{v0}^- - qV(x_n)} \left[1 - f\left(E - (E_F^{L,R} - qV^{L,R})\right)\right]dE = \int_{-\infty}^{E_{v0}^- - qV(x_n)} \frac{1}{1 + \exp\left((E_F^{L,R} - qV^{L,R}) - E/kT\right)}dE \tag{19}$$

According to Guan et al. model, the generation oxygen vacancies are given by [7]:

$$P_G(F^{eq}, T, t) = \frac{t}{t_0} \exp\left(-(E_a - \gamma|F^{eq}|)/kT\right) \tag{20}$$

where the time, t, is within the interval $[\tau, \tau + t]$, F^{eq} is the local electric field of an ion, $1/t_0 \approx 10^{13}$Hz is the oxygen vibration frequency, $E_a \approx 1$eV is a parameter related to the height of the potential barrier and γ is a coefficient which represents the local enhancement due to the electric field. This rate dominates the SET process.

On the other hand, during the equilibrium state (absence of F^{eq}), the oxygen vacancy recombination rate is given by Guan et al. [6]:

$$P_R^0 = P_G(F^{eq} = 0, T, t) = \frac{t}{t_0} \exp\left(-E_a/kT\right) \tag{21}$$

Therefore, the recombination rate for a non-equilibrium state is [7]:

$$P_R = \beta P_R^0$$

where β is a parameter related to concentration of oxygen ions which can be computed by the following approximation [6]:

$$\beta(x, t) = \beta_0 \exp\left(-\frac{vt}{L_p}\right) u(x, t) \tag{22}$$

where L_p is decaying length of ion concentration, $u(x,t)$ is a function related to the oxygen diffusion and can be approximated by the complementary error function. v is velocity of the oxygen ions waveform given by Yu et al. [7]:

$$v = \frac{a}{t_0} \exp\left(-E_m/kT\right) \sinh\left(q\gamma^{drift} F/kT\right) \tag{23}$$

where a is the lattice constant, E_m is the migration barrier, γ^{drift} is the enhancement coefficient related to the dielectric material and F is the electric field left by an oxygen ion. Eq. (13) is coupled with the solution of the Poisson equation to obtain the potential distribution in the cell:

$$-\nabla^2 V = \frac{\rho}{\varepsilon} \tag{24}$$

where ρ is the volumetric charge density and ε is the material permittivity. The border conditions for Eq. (24) are: $V(x=0)=V^L$ and $V(x=L)=V^R$. Guan et al. showed very god results of their model for experimental data of HfO_x devices [7].

4.3. Quantum point contact model

The complete quantum point contact (QPC) model was developed by Miranda and Suñe [8]. Originally, the model was developed for explaining the soft and hard-dielectric-breakdown in SiO_2. If the dimension of the narrowest point of the CF is in the order of the Fermi wavelength, λ_F, quantum point contact effects are presented. There are some experimental works, where the QPC model could explain well the transport conduction in the HRS and LRS for HfO_2 devices [9–11].

According to the QPC model, the first quantized sub-band behaves as a potential barrier for the incoming electrons as shown in **Figure 6**. We used a parabolic potential as potential barrier with the following physical parameters: Φ being the potential barrier height measured at the Fermi level, t_B is the potential thickness at the Fermi level, R is a series resistance external to the constriction, V is the applied voltage on the electrodes, q is the elementary electron charge and I is the filament current that flows in the x direction.

The potential barrier height is defined by the cross-sectional area of the constriction and determines two conduction states. For the HRS, the top of the potential barrier is above or inside the energy window and the dominant conduction mechanism is tunnelling (this description is valid only for low-voltages). On the other hand, if the top of the potential barrier is below the energy window, the cell is in the LRS and the conduction mechanism is essentially ballistic (transmission probability close to 1). The conduction in the LRS is independent of the

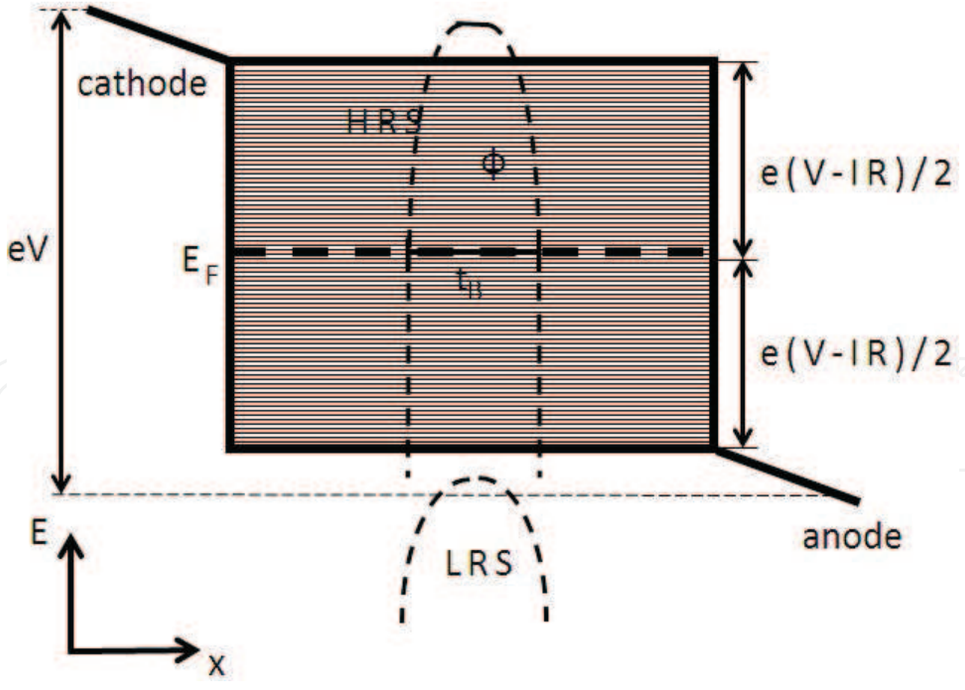

Figure 6. Energy band diagram of the narrow constriction, where V is the applied voltage on the electrodes, R is an external series resistance that takes into account the non-idealities of the model, I is the filament current, e(V-IR) is the energy window associated to the electron conduction (shaded region), EF is the Fermi level, Φ is the potential height with respect to EF, tB is the potential thickness at EF and e is the elementary electron charge. The conduction is in the x direction. The top of the potential barrier is above or inside the energy window for the HRS and below for the LRS.

potential barrier. By assuming a parabolic potential barrier in the narrow constriction and by using the Landauer formalism for 1D quantum conductors and the zero-temperature limit for the parabolic potential barrier, the current through the filament is [9, 10]:

$$I = \frac{2e}{h} N \int_{-e(V-IR)/2}^{e(V-IR)/2} T(E) dE \tag{25}$$

where $T(E)$ is the electron transmission probability, N is the number of active channels in the filament and h is the Planck's constant. For a parabolic potential barrier, there is an analytical expression for $T(E)$:

$$T(E) = \left(1 + \exp\left(-\alpha(E - \Phi)\right)\right)^{-1} \tag{26}$$

where α is a shape parameter related to t_B. By integrating over the total energy window, we have that the filament current is [9, 10]:

$$I = \frac{2eN}{h}\left\{e(V - IR) + \frac{1}{\alpha}\ln\left[\frac{1 + \exp\{\alpha[\Phi - e(V - IR)/2]\}}{1 + \exp\{\alpha[\Phi + e(V - IR)/2]\}}\right]\right\} \tag{27}$$

If we consider $V \gg IR$ and only one active filament for the HRS (not multiple filaments), we obtain [9, 10]:

$$I \approx \frac{2e}{h}\left\{eV + \frac{1}{\alpha}\ln\left[\frac{1 + \exp\{\alpha[\Phi - eV/2]\}}{1 + \exp\{\alpha[\Phi + eV/2]\}}\right]\right\} \tag{28}$$

For the LRS, we suppose an ideally ballistic transport that ($T(E) \approx 1$) and the current is [9, 10]:

$$I \approx \frac{NG_o}{1 + NG_o R} V \tag{29}$$

where $G_0 = 2q^2/h$ is the quantum conductance unit.

We show in **Figure 7** experimental results of I-V curves for the HRS and LRS and its fitting with the QPC model for HfO_2 cells. We have found in Ref. [10] that $\alpha \propto \Phi^n$ with $n = -0.35$. There is a QPC expression which relates Φ and α by considering t_B constant [9, 10]:

$$t_B = \frac{h\alpha}{2\pi^2}\sqrt{\frac{2\Phi}{m*}} \tag{30}$$

where m^* is the electron effective mass in the constriction. Moreover, the constriction radius, r_B, can be extracted by using another QPC equation [9, 10]:

$$r_B = \frac{hz_o}{2\pi\sqrt{2m * \Phi}} \tag{31}$$

where $z_0 = 2.404$ is the first zero of the Bessel function J_0. In Ref. [10], we have experimentally found that $r_B = 1.14$ nm with a standard deviation of 0.06 nm for bipolar HfO_2 cells, which

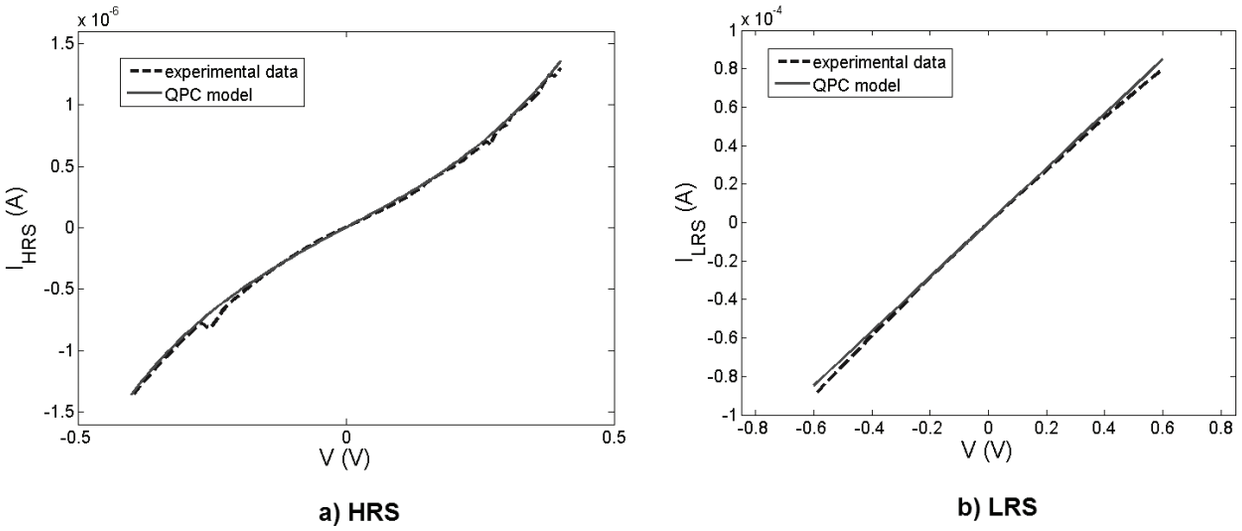

Figure 7. Experimental and theoretical I-V characteristics for the (a) HRS and (b) LRS. The QPC model (Eqs. (28) and (29)) was used for theoretical curves.

agrees with the quantum approach of this model. Miranda et al. showed that Φ has a linear dependence with respect to the temperature given by Avellán et al. [12]:

$$\Phi(T) = \Phi_0 - \gamma T \tag{32}$$

where Φ_0 is a potential height at a T_0 temperature (a given temperature) and γ is a temperature coefficient. For extracting γ, we can use the following expression [12]:

$$\frac{d(\log[I/1A])}{dT}\ln(10) = \alpha\gamma \tag{33}$$

This dependence has been probed in experimental results of HfO_2 cells in Ref. [10].

5. Conclusions

We have presented a classification of physical models for explaining the resistive switching mechanisms in chalcogonides materials. In the literature, there are many physical models proposed for explaining the electron conduction and switching mechanism in specific materials and fabrication process conditions. In the present work, we divide the models according to the number of material dimensions involved on the resistive switching mechanism. The phase change mechanism (PCM) is presented in some Te-alloys used an optical storage devices. In this switching mechanism, the material changes from the amorphous phase to the crystalline phase. Because of the resistivity affects the complete cell volume, the phase change mechanism is considered a 3D model. On the other hand, the modulation of the resistive contact is a 2D model because the defect concentration only affects the metal/insulator interface. This mechanism is presented in some perovskite materials.

The principal component of 1D models is the presence of a conduction filament. The filament is formed in a virgin cell by applying a certain threshold voltage. Depending on the cell polarity, the transport mechanisms can be: thermochemical diffusion of oxygen, filament oxidation-reduction or quantum point contact. For unipolar cells (like NiO cells), the resistive switching and the carrier conduction are controlled by the thermochemical diffusion of oxygen in the CF due to the Joule-heating effect. For bipolar cells (like HfO_2), the switching mechanism is related to the oxidation/reduction of CF. If the CF radius at the narrowest part of the CF is in the order of the Fermi wavelength, the transport is driven by the quantum point contact effect, otherwise the transport depends on the oxidation/reduction of CF.

Author details

Luis-Miguel Procel-Moya

Address all correspondence to: lprocel@usfq.edu.ec

Instituto de Micro-Nanoelectrónica, Universidad San Francisco de Quito, Quito, Ecuador

References

[1] Waser R, Wuttig M. Function by defects at the atomic scale - new concepts for non-volatile memories. In: Proceedings of ESSCIRC; IEEE.org, USA. Athens, Greece. 14–18 November 2009. pp. 65-72

[2] Wuttig M, Yamada N. Phase-change materials for rewriteable data storage. Nature Materials. 2007;**6**:824-832

[3] Sawa A. Resistive switching in transition metal oxides. Materials Today. 2008;**11**:28-36

[4] Ielmini D, Nardi F, Cagli C. Physical models of size-dependent nanofilament formation and rupture in NiO resistive switching memories. Nanotechnology. 2011;**22**:254022-1-254022-12

[5] Degraeve R, Fantini A, Raghavan N, Goux L, Clima S, Govoreanu B, Belmonte A, Linten D, Jurczak M. Causes and consequences of the stochastic aspect of filamentary RRAM. Microelectronic Engineering. 2015;**147**:171-175

[6] Guan X, Yu S, Philip Wong H -S. On the switching parameter variation of metal-oxide RRAM—Part I: Physical modeling and simulation methodology. Transactions on Electron Devices. 2012;**59**:1172-1182

[7] Yu S, Guan X, Philip Wong H-S. On the switching parameter variation of metal oxide RRAM—Part II: Model corroboration and device design strategy. IEEE Transactions on Electron Devices. 2012;**59**:1183-1188

[8] Miranda E, Suñé J. Analytic modeling of leakage current through multiple breakdown paths in SiO_2 films. In: IEEE International Proceedings Reliability Physics Symposium. IEEE.org, USA; Orlando. USA. 30 April–3 May 2001. pp. 367-379

[9] Miranda E, Walczyk C, Wenger C, Schroeder T. Model for the resistive switching effect in HfO_2 MIM structures based on the transmission properties of narrow constrictions. IEEE Electron Device Letters. 2010;**31**:609-611

[10] Procel LM, Trojman L, Moreno J, Crupi F, Maccaronio V, Degraeve R, Goux L, Simoen E. Experimental evidence of the quantum point contact theory in the conduction mechanism of bipolar HfO_2-based resistive random access memories. Journal of Applied Physics. 2012;**074509**:074509 (1-5)

[11] Degraeve R, Roussel Ph, Goux L, Wouters D, Kittl J, Altimime L, Jurczak M, Groeseneken G Generic learning of TDDB applied to RRAM for improved understanding of conduction and switching mechanism through multiple filaments. In: IEEE International Electron Devices Meeting. IEEE.org, USA; San Francisco. USA. 6–8 December 2010. pp. 632-635

[12] Avellán A, Miranda E, Schroeder D, Krautschneider W Model for the voltage and temperature dependence of the soft breakdown current in ultrathin gate oxides. Journal of Applied Physics. 2005;**014104**:014104-1-014104-5